FEBS Letters

FEBS PRESS science publishing by scientists

A mutation in *Asparagine-Linked Glycosylation 12* (*ALG12*) leads to receptor misglycosylation and attenuated responses to multiple microbial elicitors

Fabian Trempel, Lennart Eschen-Lippold, Nicole Bauer, Stefanie Ranf*, Lore Westphal, Dierk Scheel and Justin Lee

Leibniz Institute of Plant Biochemistry, Halle, Germany

Correspondence
J. Lee, Leibniz Institute of Plant Biochemistry, Weinberg 3, D-06120 Halle, Germany
Tel: +49 345 55821409
E-mail: jlee@ipb-halle.de

*** Present address**
TUM School of Life Sciences Weihenstephan, Technical University of Munich, Freising, Germany

(Received 26 November 2019, revised 11 May 2020, accepted 15 May 2020, available online 15 June 2020)

doi:10.1002/1873-3468.13850

Edited by Julian Schroeder

Changes in cellular calcium levels are one of the earliest signalling events in plants exposed to pathogens or other exogenous factors. In a genetic screen, we identified an *Arabidopsis thaliana* 'changed calcium elevation 1' (*cce1*) mutant with attenuated calcium response to the bacterial flagellin flg22 peptide and several other elicitors. Whole-genome resequencing revealed a mutation in *asparagine-linked glycosylation 12* that encodes the mannosyltransferase responsible for adding the eighth mannose residue in an α-1,6 linkage to the dolichol-PP-oligosaccharide *N*-glycosylation glycan tree precursors. While properly targeted to the plasma membrane, misglycosylation of several receptors in the *cce1* background suggests that *N*-glycosylation is required for proper functioning of client proteins.

Keywords: asparagine-linked glycosylation; calcium; membrane receptors; signalling

In addition to preformed physical barriers, pattern-triggered immunity (PTI) is one of the first lines of defence of plants against pathogen attack. This is initiated by the recognition of conserved molecular features of pathogens/microbes, so-called microbe-associated molecular patterns (MAMPs) [1,2]. MAMP recognition by cognate receptors leads to the activation of signalling cascades resulting in plant defence reactions mediated through transcriptional reprogramming of defence gene expression, as well as changes in antimicrobial metabolite and stress hormone levels. MAMPs are recognised by surface-localised receptor-like kinases (RLKs) or receptor-like proteins (RLPs). In *Arabidopsis thaliana*, the leucine-rich repeat (LRR) domain kinases, Flagellin-sensing 2 (FLS2) and elongation factor thermo unstable (EF-Tu) receptor (EFR), detect bacterial flagellin [3,4] and EF-Tu protein [5,6], respectively. The Lysin motif (LysM) domain containing RLKs Lysin motif receptor kinase 5 (LYK5) and Chitin elicitor receptor kinase 1 (CERK1) detects the fungal

Abbreviations
ALG, asparagine-linked glycosylation; BAK1, BRI1-associated kinase 1; BIK1, Botrytis-induced kinase 1; BRI1, Brassinosteroid-insensitive 1; *cce* , changed calcium elevation; CDG, congenital disorder of glycosylation; CERK, Chitin elicitor receptor kinase; CNX, calnexin; CPK, calcium-dependent protein kinase; CRT, calreticulin; DAMP, damage-associated molecular pattern; EFR, EF-Tu receptor; EF-Tu, elongation factor thermo unstable; $EndoH_f$, endoglycosidase H; ER, endoplasmic reticulum; ERAD, endoplasmic reticulum-associated degradation; ERQC, endoplasmic reticulum-based quality control; FLS2, Flagellin-sensing 2; Glc, glucose; GlcNAc, *N*-acetylglucosamine; LYK5, Lysin motif receptor kinase 5; LysM, Lysin motif; MAMP, microbe-associated molecular pattern; Man, mannose; MAPK, mitogen-activated protein kinase; OST, oligosaccharyltransferase; PDI, protein disulfide isomerase; PEPR1, Pep1-receptor 1; PNGase F, Peptide:*N*-glycosidase F; PTI, pattern-triggered immunity; RBOHD, respiratory burst oxidase homologue D; RLCK, receptor-like cytoplasmic kinase; RLK, receptor-like kinase; RLP, receptor-like protein; ROS, reactive oxygen species; SNP, single nucleotide polymorphism.

FEBS Letters **594** (2020) 2440–2451

MAMP chitin, whereas the lectin-SD-type RLK lipooligosaccharide-specific reduced elicitation is involved in the detection of bacterial medium-chain 3-hydroxy fatty acids that are derived from lipopolysaccharide [7,8]. The LRR receptors Pep1-receptor 1/2 (PEPR1/2) detect the endogenous damage signal AtPep1, which is processed and released during pathogen attack [9–13]. In order to coordinate a precise defence output, RLKs and RLPs often form complexes with coreceptors and/or auxiliary proteins. For many LRR-type RLKs or RLPs, the coreceptor is Brassinosteroid-insensitive 1 (BRI1)-associated receptor kinase 1 (BAK1) or related members from the somatic embryogenesis receptor kinase (SERK) family and/or suppressor of BIR1-1, whereas CERK1 is the coreceptor of LysM domain containing sensor proteins such as LYK5 or LYM1/3 (see [14] and references therein). Once activated, the receptor complex will initiate propagation of the immune signal. This is achieved by the phosphorylation and thus activation of receptor-like cytoplasmic kinases (RLCKs), which will in turn phosphorylate downstream targets. For example, after flagellin recognition, the BAK1-interacting Botrytis-induced kinase 1 (BIK1; an RLCK) is phosphorylated by BAK1, phosphorylates FLS2 and dissociates from the complex to phosphorylate/activate the NADPH oxidase respiratory burst oxidase homologue D (RBOHD), thereby increasing reactive oxygen species (ROS) synthesis [15–17]. Furthermore, the RLCKs have been shown to directly activate components of mitogen-activated protein kinase (MAPK) cascades, which form an important signalling branch in PTI [18,19].

Whereas signal transmission starts as a series of phosphorylation events at the receptor complex, a variety of intracellular second messengers (e.g. nitric oxide, ROS and ion currents) are indispensable to generate a timely and adequate defence output. Calcium influx into the cytosol is one of the fastest reactions after MAMP recognition [20,21] and is generated at the plasma membrane by the influx of extracellular calcium through channels formed by the cyclic nucleotide-gated channel 2/4 complexes that are also activated by BIK1-mediated phosphorylation [22]. The latter explains earlier observations of RLCKs being involved in shaping the calcium signature [23]. Apart from their role in PTI, calcium signals are known to be involved in responses to abiotic stresses as well as in the relay of developmental signals. Plants have evolved a complicated network of components involved in generating, terminating and decoding calcium signals. Intracellularly, changes in calcium levels are sensed by calcium sensors. For instance, PTI-associated calcium bursts activate signalling cascades through calcium sensors such as the calcium-dependent protein kinases (CPKs), which are required for transcriptional reprogramming of immunity-related genes and may act by directly phosphorylating transcription factors [24]. Additionally, it was shown that calcium is involved in the regulation of RBOHD in defence-related ROS production: While RBOHD is phosphorylated by BIK1, it is also regulated through direct phosphorylation by CPK5, which is activated upon rising intracellular calcium levels [25]. Furthermore, RBOHD itself is also a calcium sensor and is able to detect changes in calcium concentration via EF-hand motifs [26]. Interestingly, elevated calcium levels during tissue damage can activate the metacaspase that processes Propep1 precursor into active AtPep1 peptides [27] and thus serve to amplify immune signalling [28]. These findings illustrate the importance of calcium signals in multiple stages of early PTI signalling. In order to improve understanding of plant calcium signalling in a PTI context, we screened a mutant population for plants with a 'changed calcium elevation' (*cce*) response to MAMPs and this mainly uncovered components of the receptor complexes [29]. In similar screens based on ROS as a read-out, mutants with deficient receptor biogenesis were isolated [30]. These findings underscore a tight functional association between the receptor complex and the generation of calcium/ROS signals.

These reports also pinpoint membranes as the site for the generation of PTI-related signals: Signals are initiated at membrane-localised receptor complexes, ion fluxes are mediated through opening of transmembrane channels, and second messengers feeding back into calcium/ROS and other signalling pathways are generated at membrane-localised protein complexes. The biogenesis of transmembrane proteins and secreted proteins is a tightly controlled pathway conserved over the whole domain of eukaryotes via the endoplasmic reticulum (ER)-based quality control (ERQC) system [31]. This involves the transfer of complex glycan structures onto the asparagine residues within the *N*-linked glycosylation consensus sequence NxS/T (x = any amino acid except P, S and T) [32]. The glycans that are initially transferred in *N*-linked glycosylation share a conserved core structure of $Glc_3Man_9GlcNAc_2$ with a branched structure, consisting of lower A, middle B and upper C arms (see Fig. 3A). They are assembled in a stepwise manner on dolichol lipid anchors at the ER membrane, starting at the cytosolic side with synthesis of the mannose (Man) residues on the A arm. The glycan and its anchor are then flipped through the ER membrane, and synthesis continues at the lumenal face by addition of the Man residues to the B and C arms and finally the addition of three glucose (Glc) residues on the A arm. *N*-

acetylglucosamine (GlcNAc), Man and Glc residues are assembled by glycosyltransferases named asparagine-linked glycosylation (ALG). The resulting glycan is then transferred as a whole onto Asn residues in secreted and transmembrane proteins by the oligosaccharyltransferase (OST) complex during their translation [32,33]. The glycans of the A arm can be bound by the ER-based lectin chaperones of the ERQC pathway calnexin (CNX) and calreticulin (CRT). Binding and release of CNX and CRT are dependent on the conformation of the bound protein and are regulated by the addition or trimming of Glc residues attached to the *N*-linked glycan. After achieving its native conformation, the protein is released from the CNX/CRT pathway by trimming of the Glc residues and exported to the Golgi apparatus, where *N*-linked glycans undergo additional modifications. When a protein fails to achieve its native conformation in a given period, it undergoes Man cleavage in the C arm and thus increases the probability of interaction with lectins that remove proteins from the CNX/CRT cycle. Proteins are then retro-translocated to the cytosol and will undergo ER-associated degradation (ERAD) [34]. Mutations in *ALG* genes or in subunits of the OST complex cause drastic phenotypes in animals, but are partially tolerated in plants [35]. For instance, the *alg* mutants that showed reduced ROS or calcium response after MAMP treatment were mostly normal-looking plants [36–38]. In fact, an *alg12* mutant partially reverts the dwarf phenotype caused by mutation in the brassinosteroid receptor, BRI1 [39]. Recently, a systematic examination of multiple mutants in the *ALG* pathway showed its requirement for the cell death pathway triggered by silencing of *BAK1* and a related homologue, *SERK4* [40]. All these reports highlight the importance of proper glycosylation of *ALG* pathway client proteins for ERQC.

We previously isolated the *cce1* mutant that does not show any dramatic growth phenotype but exhibits a broad-spectrum reduced calcium response to numerous MAMPs [29]. Here, we show that *cce1* is a novel allele of *ALG12*, which encodes the α-1,6-mannosyltransferase responsible for adding the initial Man to the C arm of the glycan tree. ERQC is thus essential for proper biogenesis and functioning of MAMP receptors.

Materials and methods

Plant material, growth conditions and genotyping

An apoaequorin-expressing transgenic line, pMAQ2, was provided by Marc Knight (University of Durham), EMS-mutagenised and screened for *cce* mutants [29]. GABI-Kat collection GABI_175D12 with an insertion in *ALG12* was obtained from NASC. Plants were genotyped by PCR amplification using the following primers: ALG12-1-F (5′-CATACCACACTTCTGACTCCCCTA-3′) and ALG12-1-R (5′-GCTACAAGTAAAGACCGTGGGAGT-3′) for the wild-type ALG12 locus and with ALG12-1-R and the GABI-KAT primer o8760 (5′-GGGCTACACTGAATT-GGTAGCTC-3′) for the T-DNA insertion. Cleaved amplified polymorphic sequence (CAPS) analysis for the $ALG12^{cce1}$ single nucleotide polymorphism (SNP) was performed by *Apo*I endonuclease digestion of the PCR products amplified with the primers ALG12-CAPS-F (5′-TGGCCAAGTTTCTTCAATCC-3′) and ALG12-CAPS-R (5′-CGAGCTGCAAGACAAAATGA-3′). The DNA fragments were separated on 5% NuSieve Agarose (Biozym Scientific GmbH, Hessisch Oldendorf, Niedersachsen, Germany) gels. To generate a *cce1cce2* double mutant, crosses were made and homozygous plants were genotyped in the F2 population using the above-mentioned CAPS markers for $ALG12^{cce1}$ and $ALG3^{cce2}$ [38].

For the calcium, MAPK and qPCR assays, seeds were surface-sterilised and stratified for 2 days at 4 °C and subsequently grown in liquid MS medium for 8–10 days under long-day conditions (16-h light, 8-h dark, 21 °C) as described in Ref. [41].

Protoplast transfection, protein isolation, western blotting and endoglycosidase-based glycan analysis

Protoplasts were generated from adult (5-week-old) plants grown on soil at 22 °C under short-day conditions (8-h light, 16-h dark, 22 °C) and transfected according to the method described in Ref. [34]. After an overnight incubation (18 °C, in the dark), protoplasts were harvested by centrifugation and total proteins were isolated from protoplast pellets with extraction buffer (25 mM Tris/HCl pH 8.0, 150 mM NaCl, 1% (w/v) Nonidet P-40 and Serva Protease Inhibitor Mix P) by vigorous vortexing. After addition of 10× glycoprotein denaturation buffer (supplied with the NEB enzymes) to each sample (final conc. 1×), samples were boiled for 10 min at 100 °C and then cooled on ice. Subsequently, all samples were split into three aliquots, one was kept on ice as the 'untreated' control, and the other two were digested with Endo Hf (NEB GmbH, Frankfurt (Main), Germany) or Peptide:*N*-glycosidase F (PNGase F; NEB Inc.), respectively. Digestions were initiated by further addition of the corresponding reaction buffers (to 1×) and 2 U of Endo Hf or PNGase F and incubation at 37 °C for 1 h. Additionally, for the PNGase F digest, 1% NP40 (final concentration) was included. The digests were stopped by mixing with standard SDS/PAGE sample loading buffer and separated on 8% standard SDS/PAGE. Gels were blotted onto Porablot NCL nitrocellulose membranes

(Macherey-Nagel), and proteins were detected by western blot using Living Colors® GFP Monoclonal Antibody (Takara Bio Europe, Saint-Germain-en-Laye, France) and anti-mouse IgG-HRP (Sigma-Aldrich, Munich, Germany) according to the manufacturer's protocols.

Gene expression analysis

For gene expression analysis, pools of fifteen 8-day-old seedlings of the indicated plant lines were flash-frozen and RNA was extracted. RNA extraction, cDNA synthesis and qPCR were performed as described in Ref. [42]. *ALG12* expression was normalised to expression of *PP2A*. The primer pairs used are as follows: *ALG12* (5′-TGAAGATGATTTTCCGTGGAG-3′ and 5′-CAGAGGAATGCTGTTCACC-3′); *PP2A* (5′-GACCGGAGCCAACTAGGAC-3′ and 5′-AAAACTTGGTAACTTTTCCAGCA-3′).

Calcium measurements

Calcium measurements of 8- to 10-day-old pMAQ2 seedlings were performed as described in Ref. [29,41] and converted into intracellular calcium concentration [43].

Confocal microscopy

Microscopic analysis of fluorescence-tagged receptor and coreceptors expressed in mesophyll protoplasts was performed as described previously [38]. Briefly, after an overnight incubation (~ 16 h) period to enable protein expression, protoplasts were observed on a LSM 710 confocal laser scanning microscope (Carl Zeiss, Jena, Germany), with the following excitation settings (GFP: 488 nm; YFP: 514 nm). Acquired images (ZEN 2012 software; Carl Zeiss) were processed with IMAGEJ software (National Institute of Health, Bethesda, MD, USA).

Statistical analysis

Statistical analyses were performed with the GraphPad Prism 5 (San Diego, CA, USA) software package with the tests specified in the respective figure legends.

Results

cce1 has a broad-spectrum calcium signalling phenotype (similar to *cce2*) but is not allelic to *cce2*

The '*cce*' mutant, *cce1*, was reported to exhibit reduced response to a number of elicitors (but note that the actual calcium traces were not shown) [29]. Here, we validated the attenuated calcium response to several peptide elicitors (flg22, elf18 and pep1) or chitin as compared to the parental line, pMAQ2. By integrating the 'area under the curve (AUC)' as quantification of the total response, the *cce1* mutant shows a ~ 7–20% reduction in its calcium response to the tested elicitors (Fig. 1). This indicates a perturbation of multiple signalling pathways, as not only the FLS2/EFR/PEPR1-BAK1 receptor complexes involved in peptide MAMP recognition, but also the CERK1/LYK5 complexes involved in the sensing of chitin are disturbed. To exclude a general effect on calcium influxes, we tested an abiotic stress (200 mM NaCl treatment), where the salt stress-induced calcium response was not reduced, but rather mildly enhanced, in the *cce1* mutant (Fig. S1). Hence, the reduced calcium response seems to be specific to the tested biotic signals. This broad-spectrum *cce1* phenotype to multiple biotic stress signals resembles that of a previously characterised *cce2* mutant [38] and suggests that like *cce2*, the *cce1* mutation(s) may affect a global function relevant for the different receptors.

To check for epistasis or allelism, *cce1* was previously crossed with *bak1-4 or cce2*, where the attenuated flg22-induced calcium response of the *cce1* mutant was restored to wild-type level in the F1 generation [29], suggesting that it is not allelic to the *BAK1* coreceptor or the *CCE2* gene, respectively. *cce2* and the allelic *cce3* are different mutants of *ALG3*, a mannosyltransferase involved in ER quality control via *N*-linked glycosylation [38] (see Fig. 3A for scheme of ALG pathway). As any perturbation of this pathway will affect all transmembrane proteins harbouring *N*-linked glycosylation sites in their exoplasmic domains, most receptors will be globally affected. Thus, we wondered whether *cce1* may be mutated in the same pathway as *cce2*/*cce3* and generated a *cce1cce2* double mutant to test this hypothesis. When treated with flg22, the *cce1cce2* double mutant exhibited a calcium phenotype similar to the *cce1* or *cce2* single mutations. From the AUC analysis, the mutants possess 83–89% of the wild-type calcium response but are not statistically different between themselves (Fig. 2A).

Mitogen-activated protein kinase activation is one of the earliest signalling events downstream of calcium influx and can be visualised by a western blot-based detection of the phosphorylated MAPK proteoforms. Three phospho-MAPK bands are typically detected after flg22 elicitation. Using the Odyssey quantitative western blot analysis system (LI-COR Bioscience), we calculated the total signal intensities of all three bands (at 15 min postelicitation). Compared to the pMAQ2 parental plants, flg22-induced MAPK activation is attenuated in *cce1*, *cce2* and *cce1cce2* double mutant (Fig. 2B). Similar to the calcium response, there is no

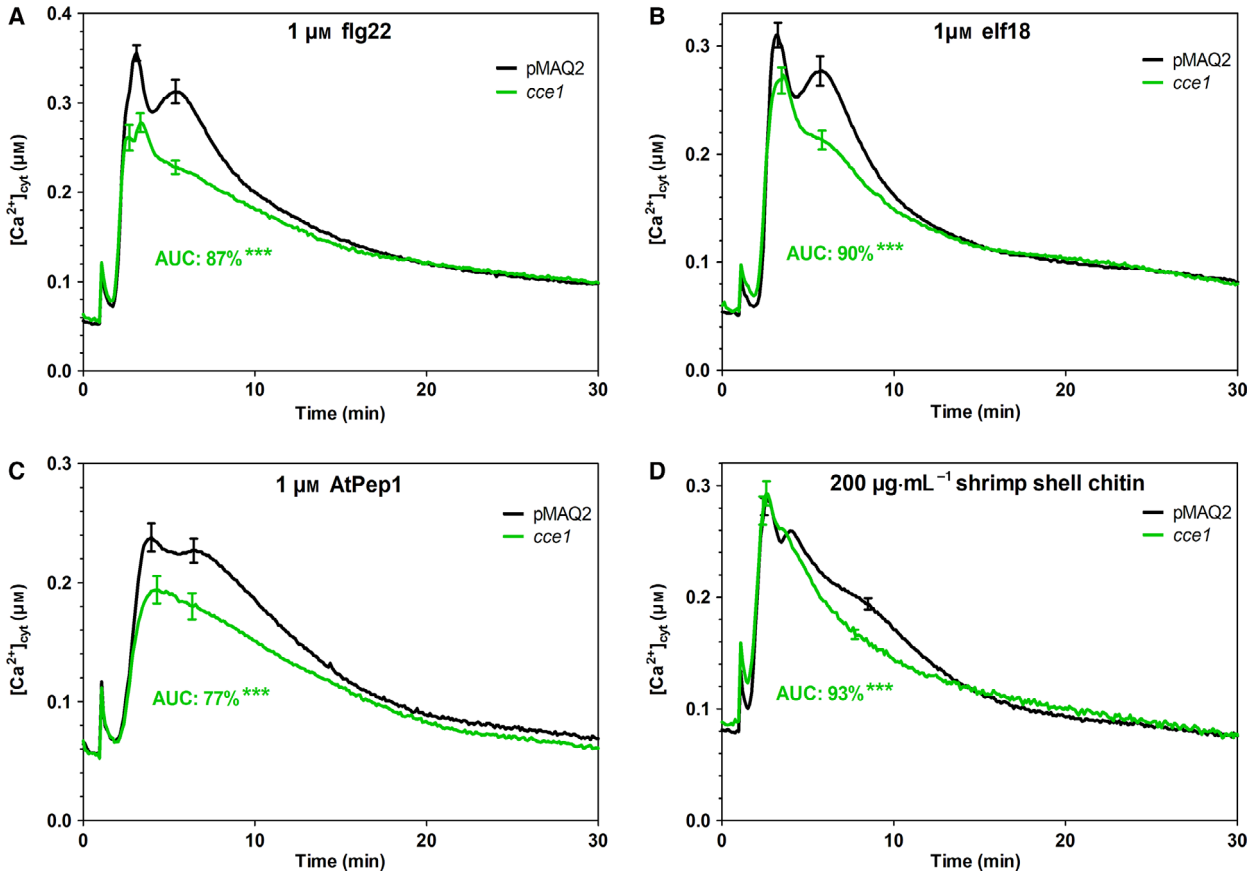

Fig. 1. *cce1* is a broad-spectrum calcium signalling mutant. Calcium signatures of *cce1* compared with the parental line pMAQ2 (expressing the calcium reporter aequorin). Eight- to 10-day-old seedlings were treated with the indicated bacterial MAMPs flg22 (A) and elf18 (B), the DAMP AtPep1 (C) or shrimp shell chitin (D). Error bars represent 95% confidence intervals (n = 21, 21, 33 or 39 for flg22, elf18, AtPep1 or chitin, respectively). AUC was used to quantify the 'total calcium response within 30 min of elicitor treatment' and calculated as per cent of the pMAQ2 signal (set as 100%). ***$P < 0.001$ (paired t-test comparison between *cce1* and pMAQ2).

additive effect of stacking *cce1* and *cce2* mutations, with the MAPK activation in the double mutant being comparable to the response in *cce1* or *cce2* (Fig. 2B). These results suggest that the two mutations may indeed affect the same pathway.

cce1 is a novel allele of *ALG12*

Whole-genome resequencing was performed on the *cce1* mutant, and 35 nonsynonymous mutations were identified (Table S1). Among the candidates, a putative SNP in a mannosyltransferase gene (AT1G02145) was detected, which was validated by resequencing and CAPS (cleaved amplified polymorphic sequence) analysis (see Materials and methods). This C-to-T mutation leads to a T70I exchange in the encoded ALG12 protein (Fig. 3A, B). A mutant of *ALG12* had been previously isolated in an 'EMS-mutagenised brassinosteroid receptor 1 suppressor (*ebs*)' screen, with the SNP in the *ebs4-3* mutant leading to an E38K exchange located in a predicted ER lumen-localised protein loop [35]. As illustrated by the alignment with several plant orthologues and the human ALG12 (Fig. 3B), the T70I exchange caused by the *cce1* mutation is located in this same luminal loop, which is highly conserved between plants, fungi and animals. Fortuitously, a human T67M exchange at the corresponding orthologous T70 position has been identified in patients with congenital disorder of glycosylation (CDG), a severe disease with multisystem defects [44]. Since the human $ALG12^{T67M}$ allele failed to complement *alg12* in yeast, the $ALG12^{T70I}$ allele isolated here is likely to also encode mannosyltransferase with reduced or impaired activity.

In order to validate the causal relationship of the T70I mutation in *ALG12* and the calcium phenotype

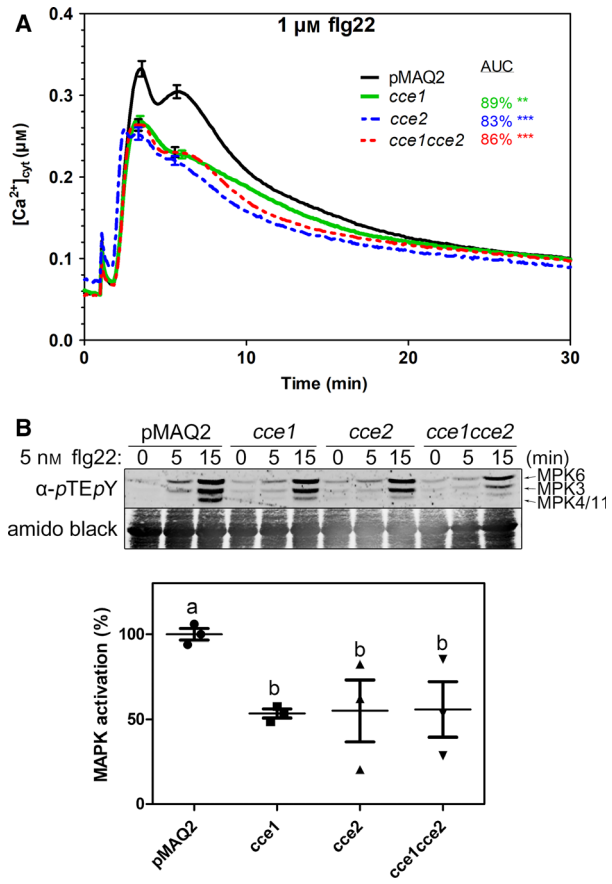

Fig. 2. Attenuated response of *cce1* is not increased in the *cce1cce2* double mutant. (A) Flg22-induced calcium elevations in *cce1*, *cce2* and the double mutant line *cce1cce2*. Error bars represent 95% confidence intervals ($n = 88$ for all except *cce2*, where $n = 32$). The per cent AUC compared to pMAQ2 is shown (**$P < 0.01$, ***$P < 0.001$, one-way ANOVA). (B) Flg22-induced MAPK activation was monitored using an antibody that recognises phosphorylated MAPKs (α-*p*TE*p*Y). Leaf material was harvested at the indicated time points after infiltration of flg22 (5 nM) and processed for quantitative western blotting with the Odyssey Infrared Imaging System (LI-COR Biosciences, Lincoln, NE, USA). Linearity of the assay was validated using a serial dilution (see Fig. S2). Total signal intensity of all three immunoreactive MAPK bands was normalised against the total proteins (Revert 700 Total Stain; LI-COR) and used as an estimation of total flg22-induced MAPK activation (at 15 min). Three independent biological replicates were processed, and all values were normalised against pMAQ2 (with the average signals set as 100 %). Alphabets mark the distinct statistically significant groups (one-way ANOVA). Mean (horizontal line) and SD (error bars) are included in the scatter plot.

in *cce1*, crosses were performed with a T-DNA insertion line (GABI_175D12 from the GABI-KAT collection), hereafter designated as *alg12-T*. Unfortunately, no homozygous *alg12-T* was recovered from the segregating GABI-Kat line, indicating that homozygous *alg12-T* may be lethal. Thus, *cce1* was crossed to a heterozygous *alg12-T* line. Out of 20 F1 plants screened, only one heterozygous *cce1 alg12-T* plant was recovered, thus supporting the notion of reduced fitness of plants bearing the *alg12-T* allele. The segregating F2 population of this heterozygous *cce1 alg12-T* plant was genotyped for both the *cce1* SNP and the T-DNA insertion in *ALG12*. Only homozygous *cce1* individuals or heterozygous *cce1 alg12-T* plants were recovered (Fig. 3C). The calcium response to flg22 treatment in this pool of F2 segregants from the *cce1 alg12-T* heterozygous line is indistinguishable from that of the *cce1* mutant (Fig. 3D). Thus, from this allelism analysis, *alg12-T* does not complement *cce1* and supports the notion that *alg12* is the causal mutation for the *cce1* phenotype.

Receptor localisation is unaltered in *cce1*

Previous studies have suggested that mutations in genes of the *ALG* pathway lead to a reduction in ERQC stringency, allowing mutated and malformed proteins to reach the plasma membrane, which would otherwise be targeted for ERAD [35]. To check whether receptors are correctly targeted to the plasma membrane in *cce1* and *cce1cce2* double mutant lines, we analysed protoplasts transiently expressing fluorescent protein-tagged FLS2, EFR, PEPR1 or CERK1 receptors. Most of the fluorescence signals were present in the cell periphery, suggesting correct targeting of receptors to the plasma membrane (Fig. 4A). We had previously reported that whereas *cce2* and *cce3* harbour slightly less endogenous FLS2 than the parental line [38], this was not the case for *cce1* [29]. Here, anti-GFP antibodies were used to check protein levels of the various GFP- or YFP-tagged receptor proteins in the *cce* background, but unfortunately, inconsistent transfection efficiencies between samples precluded this comparison. However, most of the receptors expressed in the *cce1*, *cce2* or *cce1cce2* double mutant background show a faster migration pattern in the SDS/PAGE (Fig. 4B). An exception is CERK1 that showed little-to-no difference in the *cce1* background when compared to the pMAQ2, but as reported previously, enhanced mobility of CERK1 can be discerned in the *cce2* background [38] or also here, with a shorter exposure of the western blot (last panel on the right of Fig. 4B). Thus, the observation of receptors with altered sizes is in line with ALG12 mutation leading to misglycosylation.

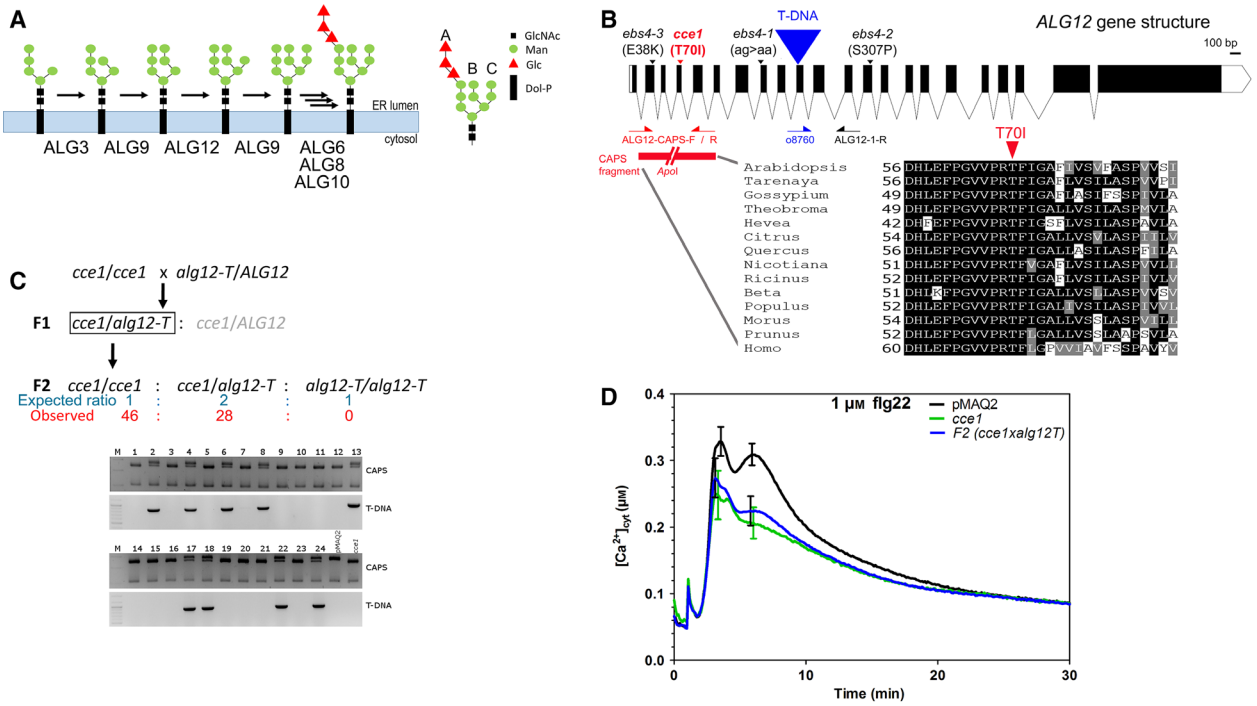

Fig. 3. *cce1* is mutated in *ALG12*. (A) Scheme of the relevant part of *Arabidopsis thaliana* ALG pathway for $Glc_3Man_9GlcNAc_2$ synthesis. For simplicity, only synthesis steps on the lumenal face of the ER membrane are shown. (B) Gene structure of the Arabidopsis *ALG12* gene and position of mutations (*cce1* and previously published *ebs4* mutants). Exons are represented by black blocks. Positions of primers used for genotyping are indicated by arrows. The alignment shows the conservation of the region spanning the T70I exchange in selected plant species and the human *ALG12*. (C) Scheme of the genetic analysis of a cross between the *cce1* mutant and a plant heterozygous for an *alg12* T-DNA insertion. To genotype the offspring from a *cce1 alg12-T* heterozygous F1 plant (highlighted by box), PCR was performed using the primers indicated in (B). Top panels: For CAPS analysis, the PCR products were digested with *Apo*I, resulting in 481 and 307 bp fragments for wild-type sequence or 454, 307 and 29 bp fragments for the *cce1* sequence (note that the 29 bp fragment is not visible on this gel). Bottom panels: Gels showing the absence/presence of amplicons diagnostic for the *alg12* T-DNA insertion. Note that no plants homozygous for the T-DNA insertion could be identified. The representative gels shown are taken from a single experiment with $n = 24$. Two further experiments were performed and the pooled results used to compute the observed segregation ratio. (D) Calcium elevation in response to flg22 treatment (1 µM) in the F2 segregants described in panel C (Note that this represents a mix of *cce1* homozygotes and *cce1alg12-T* heterozygotes). Error bars represent the 95% confidence interval ($n = 36$ for pMAQ2 or *cce1* and 93 for the F2 pool).

Receptor glycosylation is compromised in *cce1*

Levels of the endogenous *ALG12* mRNAs are not compromised in the *cce1* or *cce1cce2* double mutants (Fig. 5A). Hence, the *cce1* phenotype is not due to reduced expression at the transcript level. If the hypomorphic $T70I^{cce1}$ mutation results in a less efficient mannosyltransferase activity of ALG12, then glycosylated proteins with extracellular domains should consequently exhibit aberrant sizes, which is consistent with enhanced electrophoretic mobility for FLS2, EFR and PEPR1 when expressed in the *cce1*, *cce2* and the *cce1cce2* double mutant background. For CERK1, the poor gel resolution did not permit clear conclusion on size differences in *cce1* although it is indeed smaller in the *cce2* background (Fig 4B and [38]).

To compare the receptor glycosylation status in the *cce* mutants, we selected FLS2-YFP as a representative for further analysis. Deglycosylation assays were performed on membrane proteins prepared from the different genotypes. Upon treatment with PNGase F (an amidase that cleaves the linkage between GlcNAc and the Asn), YFP-tagged FLS2 expressed in the different lines mostly ran as a species of approximately 190 kDa, suggesting that the observed differences in running behaviour (compared to the wild-type) are indeed caused by different glycan structures. The partial cleavage of FLS2 expressed in the mutants may reflect poorer accessibility of PNGase F due to differentially glycosylated receptors.

By contrast, receptors expressed in *cce2* and the *cce1cce2* double mutant were completely resistant to

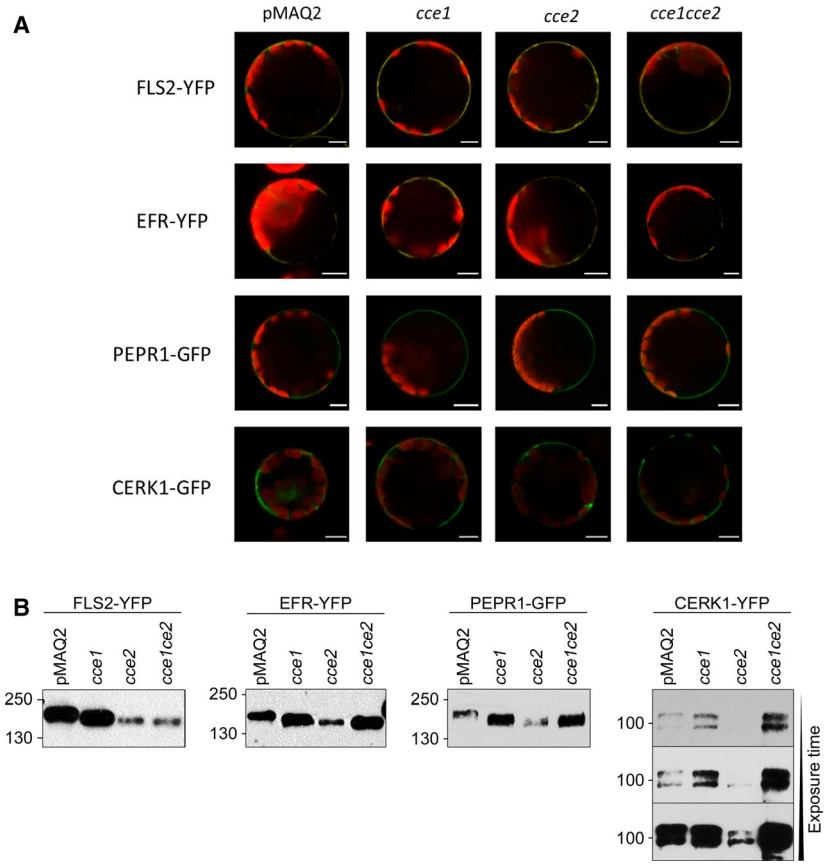

Fig. 4. Receptor localisation is unaltered in *cce1 or cce2* mutants, but the proteins have altered migration in SDS/PAGE. YFP- or GFP-tagged receptors were transiently expressed in protoplasts generated from pMAQ2, *cce1*, *cce2* or the double mutant. (A) Confocal images of the protoplasts showing the resulting receptor signals mostly in the cell periphery (likely plasma membrane) in all cases. Chlorophyll autofluorescence (red) is included to show positions of the chloroplasts. Scale bars represent 10 μM. (B) Western blot with anti-GFP antibodies. For CERK1, multiple exposures of the western blot are shown to visualise the low levels in some samples. Numbers on the left mark the position of molecular weight markers.

cleavage by endoglycosidase H ($EndoH_f$), whereas FLS2 expressed in *cce1* was partially deglycosylated. The former is compatible with the notion that $EndoH_f$ does not cleave low-Man glycan trees [45] and the glycan trees in the *cce2* background would contain only five Man units (see scheme in Fig. 3A). Glycans in *cce1* background are predicted to contain seven Man units and are cleavable by $EndoH_f$. Taken together with the enhanced mobility, several of the receptors expressed in the *cce1* background are underglycosylated.

Discussion

We identified a calcium response mutant, *cce1*, with attenuated response to several MAMPs and damage-associated molecular patterns (DAMPs), which acts in the same genetic pathway as *ALG3*. The corresponding *cce1* mutation was identified to reside in *ALG12*, which encodes the α-1,6-mannosyltransferase that acts two steps downstream of ALG3 in the *N*-linked glycosylation pathway (see Fig. 3A). Mutations in *ALG12* (designated as *ebs4*) have previously been described in a brassinolide signalling context for biogenesis of the BRI1 receptor. As shown in sequence alignment (Fig 3B), the E38K mutation that abrogates $ALG12^{ebs4\text{-}3}$ function [35] lies in the same ER luminal protein loop as the $T70I^{cce1}$ exchange (which is equivalent to the human CDG disease-associated $T67M^{CDG}$ exchange [44]). Thus, this protein loop is likely to be important for its function. As the *cce1* mutation did not lead to lowered $ALG12^{T70I}$ mRNA levels, the phenotype can be attributed to impaired protein function leading to the production of aberrant glycan structures.

Crosses of *cce1* with a T-DNA insertion line for *ALG12* (*alg12-T*) support the interpretation that *alg12*

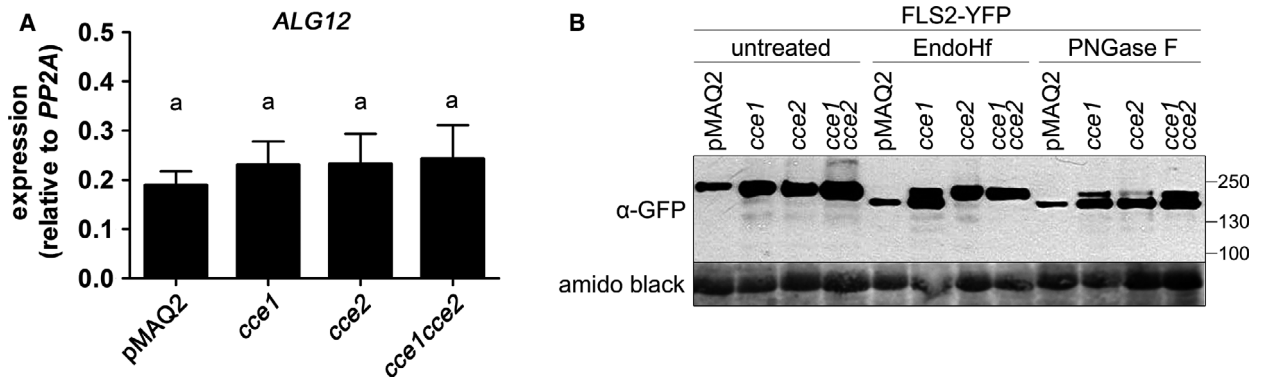

Fig. 5. *ALG12* transcript levels are unaffected in the *cce1* mutant, but FLS2 expressed in the *cce1* background is partially resistant to EndoHf deglycosylation. (A) RT-qPCR expression analysis of *ALG12* in mutant lines and the parental line pMAQ2. *ALG12* expression is not reduced in mutant lines. Error bars represent standard deviation ($n = 4$). Statistical significance is indicated by the alphabets above each bar (one-way ANOVA, Neumann–Keuls multiple comparison *post hoc* test, $P < 0.05$). (B) Comparison of receptor deglycosylation patterns in different genotypes. FLS2-YFP was transiently expressed in the indicated genotype, and extracted membrane proteins were subjected to deglycosylation with EndoHf or PNGase F and processed for western blotting. Molecular size markers are indicated on the right, and amido black staining is included as loading control.

accounts for the observed calcium signalling phenotype. The genetic analysis was complicated by the failure to isolate homozygous *alg12-T* plants, suggesting the T-DNA insertion likely creates a null and lethal allele. Indeed, besides not obtaining homozygous *alg12-T* plants in the offspring from the heterozygous *cce1 alg12-T* line, a non-Mendelian segregation pattern was observed. Contrary to the expected 1 : 2 ratio of *cce1* homozygotes and *cce1 alg12-T* heterozygotes (if *alg12-T* homozygotes were nonviable), an approximate 2 : 1 ratio (i.e. 46 *cce1* homozygotes:28 *cce1 alg12-T* heterozygotes) was obtained (Fig. 3C). This ratio inversion is indicative of *alg12-T* heterozygous plants having reduced fitness (that may lead to conditional lethality). Analogously, this is in agreement with the severe developmental defects and psychomotor retardation manifested in a patient heterozygous for the $ALG12^{T67M}$ allele and a second $ALG12^{R146Q}$ allele [44]. Nevertheless, since another $ALG12^{ebs4\text{-}1}$ aberrant splicing allele that results in premature translational termination was previously identified [35], null alleles of *alg12* may not necessarily be lethal and we cannot fully exclude that lethality of the *alg12-T* allele may be caused by a closely linked gene. Similarly, the *cce1* mutant contains additional mutations that may contribute to the calcium response. For instance, it has seven putative nonsynonymous SNPs on the same chromosome as *ALG12* (Table S1), albeit the closest is ~ 1 million bp away. Thus, although the allelism analysis involving the F2 population of the *cce1*x*alg12-T* cross is good genetic evidence that the altered flg22-induced calcium phenotype is due to *ALG12*, further validation should be obtained in the future by genetic complementation specifically with the *ALG12* locus.

In accordance with hampered mannosyltransferase activity, receptors expressed in mutant-derived protoplasts show a different separation pattern in SDS/PAGE, most likely caused by occupancy of glycosylation sites with aberrant glycans. Consistent with the proposed function of ALG12 and previous glycan analyses on *alg12*, receptors expressed in *cce1* background contain high-Man glycans that can be partially removed by $EndoH_f$ in contrast to receptors expressed in *alg3* lines. Remarkably, the proposed glycan structures in *alg12* and *alg3* only differ in the presence of two Man residues on the B-arm of the glycan but still result in differential cleavage by Endo H_f. As receptors expressed in the mutant lines mostly migrated as single species, *cce1* appears to lead to complete residence of glycosylation sites, albeit with aberrant glycans, as described previously [46]. This is in contrast to *alg* phenotypes in yeast, where malformed glycans are transferred with less efficiency by the OST, leading to incomplete glycosylation site occupancy [33].

Receptor localisation was unaltered in *cce1*, which is in accordance with the phenotypes in *ebs4*, which renders ERQC less stringent for misglycosylated receptors [35]. We had previously found that receptor levels of FLS2 were not reduced in *cce1* compared to wild-type plants, whereas receptor levels were reduced in *cce2* [29]. We, however, cannot determine whether this translates into different mechanisms behind the observed mutant phenotypes or whether lacking ERQC will always lead to faulty calcium signalling

independently from receptor levels. In this connection, we could not clearly clarify if the CERK1 receptors are differentially glycosylated in *cce1* although it is underglycosylated in the *cce2* background (Fig 4B), thus questioning if the minor reduction in calcium response to chitin is indeed linked to compromised receptor function in *cce1*. Notably, the chitin-induced response in *cce1* showed a loss of the 'shoulder region' of the calcium response curve (Fig 1D), which is reminiscent to that seen in the *rbohD* mutant or after inhibition of ROS production by treatment with the NADPH oxidase inhibitor, diphenyleneiodonium [20]. Thus, although glycosylation of plant RBOHD has not been reported, it is tempting to speculate that RBOHD misglycosylation may contribute to the altered calcium response in *cce1*. By analogy, human NOX1 NADPH oxidase is *N*-glycosylated at N162 and N236 but their mutations have no impact on surface localisation [47]. Taken together, other *N*-linked glycosylation client proteins that are relevant for the pathway, for example BAK1 [40] or potentially also the calcium channels, will influence calcium response in most *alg* mutants.

Along the same line of argument, receptor biogenesis has long been described as an important factor in proper response of plants to external stimuli. Due to the conserved role of *N*-linked glycosylation in ERQC, glycosylation mutants have been discovered in screens for various signalling pathways in plants. Consequentially, calcium signalling is affected by ERQC pathway mutants as are other signalling pathways that rely on exoplasmic or transmembrane glycosylated protein components. The affected pathways are diverse and so are the consequences of mutations in *N*-linked glycosylation. Whereas mutations in *ALG3* have been shown to lead to reduced numbers of receptors in the plasma membrane [29,38], *ALG12* mutations have been linked to a less stringent ERQC allowing for mutated receptors to reach the plasma membrane which would otherwise be trapped in the ER [35,39,48]. In human cell lines, faulty *N*-linked glycosylation was shown to alter re-internalisation kinetics of a G protein-coupled receptor [44]. In plant *N*-glycosylation mutants, the EFR receptor was shown to lose ligand binding and display reduced plasma membrane accumulation and interaction with its coreceptor BAK1 [49]. The manifold possible consequences of lacking glycosylation and the often cryptic phenotypes impede the identification of causal relations between mis- or underglycosylation and the observed phenotypes. This is aggravated by the fact that different proteins show different reactions for similar glycan aberrations and even different glycosylation sites on the same protein fulfil different functions. In order to uncover the functional relevance of lacking glycosylation, components of the receptor complexes and downstream signalling components need to be studied separately.

In summary, when the findings in this report are taken in context with our *cce* screen [29,38], the recurrent isolation of components of receptor complexes or elements required for proper receptor biogenesis when using calcium response as a read-out during genetic screens shows that quantitative calcium measurement is a good proxy for function of receptors and surface components.

Acknowledgements

We thank Christiane Förster for student assistantship and Julia Grimmer for initial allelism analysis. Silke Robatzek and Yusuke Saijo kindly provided the vectors for expressing GFP/YFP-tagged MAMP receptors; Marc Knight provided the original pMAQ2 apoaequorin-expressing line that we used for EMS mutagenesis. This work is supported by grants from the German Research Foundation (DFG) within the SPP1212 Priority Program (grant number: LE2321/1-3) and in part by grant number LE2321/3-1, as well as core funding of our institute (Leibniz Foundation). The funding sources are not involved in the study design, data collection/interpretation or decision to submit the publication.

Author contributions

FT, LE-L, NB and LW designed and performed the experiments. SR isolated the *cce* mutants and was involved in initial genetic mapping, whole-genome sequencing and mutant characterisation together with LW. DS and JL supervised the project. FT and JL wrote the paper with contribution from all authors.

Conflicts of interest

The authors have no conflict of interest to declare regarding this submission.

References

1 Jones JD and Dangl JL (2006) The plant immune system. *Nature* **444**, 323–329.
2 Dodds PN and Rathjen JP (2010) Plant immunity: towards an integrated view of plant-pathogen interactions. *Nat Rev Genet* **11**, 539–548.
3 Gómez-Gómez L, Bauer Z and Boller T (2001) Both the extracellular leucine-rich repeat domain and the

kinase activity of FSL2 are required for flagellin binding and signaling in *Arabidopsis*. *Plant Cell* **13**, 1155–1163.
4 Gómez-Gómez L, Felix G and Boller T (1999) A single locus determines sensitivity to bacterial flagellin in *Arabidopsis thaliana*. *Plant J* **18**, 277–284.
5 Kunze G, Zipfel C, Robatzek S, Niehaus K, Boller T and Felix G (2004) The N terminus of bacterial elongation factor Tu elicits innate immunity in *Arabidopsis plants*. *Plant Cell* **16**, 3496–3507.
6 Zipfel C, Kunze G, Chinchilla D, Caniard A, Jones JDG, Boller T and Felix G (2006) Perception of the bacterial PAMP EF-Tu by the receptor EFR restricts Agrobacterium-mediated transformation. *Cell* **125**, 749–760.
7 Kutschera A, Dawid C, Gisch N, Schmid C, Raasch L, Gerster T, Schäffer M, Smakowska-Luzan E, Belkhadir Y, Vlot AC *et al*. (2019) Bacterial medium-chain 3-hydroxy fatty acid metabolites trigger immunity in *Arabidopsis* plants. *Science* **364**, 178–181.
8 Ranf S, Gisch N, Schäffer M, Illig T, Westphal L, Knirel YA, Sánchez-Carballo PM, Zähringer U, Hückelhoven R, Lee J and *et al*. (2015) A lectin S-domain receptor kinase mediates lipopolysaccharide sensing in *Arabidopsis thaliana*. *Nat Immunol* **16**, 426–433.
9 Huffaker A, Pearce G and Ryan CA (2006) An endogenous peptide signal in *Arabidopsis* activates components of the innate immune response. *Proc Natl Acad Sci USA* **103**, 10098–10103.
10 Krol E, Mentzel T, Chinchilla D, Boller T, Felix G, Kemmerling B, Postel S, Arents M, Jeworutzki E, Al-Rasheid KAS *et al*. (2010) Perception of the *Arabidopsis* danger signal peptide 1 involves the pattern recognition receptor AtPEPR1 and its close homologue AtPEPR2. *J Biol Chem* **285**, 13471–13479.
11 Yamaguchi Y, Huffaker A, Bryan AC, Tax FE and Ryan CA (2010) PEPR2 is a second receptor for the Pep1 and Pep2 peptides and contributes to defense responses in *Arabidopsis*. *Plant Cell* **22**, 508–522.
12 Yamaguchi Y, Pearce G and Ryan CA (2006) The cell surface leucine-rich repeat receptor for AtPep1, an endogenous peptide elicitor in *Arabidopsis*, is functional in transgenic tobacco cells. *Proc Natl Acad Sci USA* **103**, 10104–10109.
13 Qi Z, Verma R, Gehring C, Yamaguchi Y, Zhao Y, Ryan CA and Berkowitz GA (2010) Ca2+ signaling by plant *Arabidopsis thaliana* Pep peptides depends on AtPepR1, a receptor with guanylyl cyclase activity, and cGMP-activated Ca2+ channels. *Proc Natl Acad Sci USA* **107**, 21193–21198.
14 Couto D and Zipfel C (2016) Regulation of pattern recognition receptor signalling in plants. *Nat Rev Immunol* **16**, 537–552.
15 Lu D, Wu S, Gao X, Zhang Y, Shan L and He P (2010) A receptor-like cytoplasmic kinase, BIK1, associates with a flagellin receptor complex to initiate plant innate immunity. *Proc Natl Acad Sci USA* **107**, 496–501.
16 Kadota Y, Sklenar J, Derbyshire P, Stransfeld L, Asai S, Ntoukakis V, Jones JDG, Shirasu K, Menke F, Jones A and *et al*. (2014) Direct regulation of the NADPH oxidase RBOHD by the PRR-associated kinase BIK1 during plant immunity. *Mol Cell* **54**, 43–55.
17 Li L, Li M, Yu L, Zhou Z, Liang X, Liu Z, Cai G, Gao L, Zhang X, Wang Y *et al*. (2014) The FLS2-associated kinase BIK1 directly phosphorylates the NADPH Oxidase RbohD to control plant immunity. *Cell Host Microbe* **15**, 329–338.
18 Yamada K, Yamaguchi K, Shirakawa T, Nakagami H, Mine A, Ishikawa K, Fujiwara M, Narusaka M, Narusaka Y, Ichimura K *et al*. (2016) The *Arabidopsis* CERK1-associated kinase PBL27 connects chitin perception to MAPK activation. *EMBO J* **35**, 2468–2483.
19 Rao S, Zhou Z, Miao P, Bi G, Hu M, Wu Y, Feng F, Zhang X and Zhou J-M (2018) Roles of receptor-like cytoplasmic kinase VII members in pattern-triggered immune signaling. *Plant Physiol* **177**, 1679–1690.
20 Ranf S, Eschen-Lippold L, Pecher P, Lee J and Scheel D (2011) Interplay between calcium signalling and early signalling elements during defence responses to microbe- or damage-associated molecular patterns. *Plant Journal* **68**, 100–113.
21 Seybold H, Trempel F, Ranf S, Scheel D, Romeis T and Lee J (2014) Ca^{2+} signalling in plant immune response: from pattern recognition receptors to Ca^{2+} decoding mechanisms. *New Phytol* **204**, 782–790.
22 Tian W, Hou C, Ren Z, Wang C, Zhao F, Dahlbeck D, Hu S, Zhang L, Niu Q, Li L *et al*. (2019) A calmodulin-gated calcium channel links pathogen patterns to plant immunity. *Nature* **572**, 131–135.
23 Ranf S, Eschen-Lippold L, Fröhlich K, Westphal L, Scheel D and Lee J (2014) Microbe-associated molecular pattern-induced calcium signaling requires the receptor-like cytoplasmic kinases, PBL1 and BIK1. *BMC Plant Biol* **14**, 374.
24 Hake K and Romeis T (2019) Protein kinase-mediated signalling in priming: Immune signal initiation, propagation, and establishment of long-term pathogen resistance in plants. *Plant, Cell Environ* **42**, 904–917.
25 Dubiella U, Seybold H, Durian G, Komander E, Lassig R, Witte C-P, Schulze WX and Romeis T (2013) Calcium-dependent protein kinase/NADPH oxidase activation circuit is required for rapid defense signal propagation. *Proc Natl Acad Sci USA* **110**, 8744–8749.
26 Kadota Y, Shirasu K and Zipfel C (2015) Regulation of the NADPH oxidase RBOHD during plant immunity. *Plant Cell Physiol* **56**, 1472–1480.
27 Hander T, Fernández-Fernández ÁD, Kumpf RP, Willems P, Schatowitz H, Rombaut D, Staes A, Nolf J,

Pottie R, Yao P *et al.* (2019) Damage on plants activates Ca(2+)-dependent metacaspases for release of immunomodulatory peptides. *Science* **363**, eaar7486.
28 Huffaker A and Ryan CA (2007) Endogenous peptide defense signals in *Arabidopsis* differentially amplify signaling for the innate immune response. *Proc Natl Acad Sci USA* **104**, 10732–10736.
29 Ranf S, Grimmer J, Pöschl Y, Pecher P, Chinchilla D, Scheel D and Lee J (2012) Defense-related calcium signaling mutants uncovered via a quantitative high-throughput screen in *Arabidopsis thaliana*. *Molecular Plant* **5**, 115–130.
30 Segonzac C and Zipfel C (2011) Activation of plant pattern-recognition receptors by bacteria. *Curr Opin Microbiol* **14**, 54–61.
31 Drummond DA and Wilke CO (2009) The evolutionary consequences of erroneous protein synthesis. *Nat Rev Genet* **10**, 715–724.
32 Aebi M (2013) N-linked protein glycosylation in the ER. *Biochim Biophys Acta Mol Cell Res* **1833**, 2430–2437.
33 Burda P and Aebi M (1999) The dolichol pathway of N-linked glycosylation. *Biochem Biophys Acta* **1426**, 239–257.
34 Liu Y and Li J (2014) *Endoplasmic reticulum-mediated protein quality control in Arabidopsis*. *Front Plant Sci* **5**. 162.
35 Hong Z, Jin H, Fitchette A-C, Xia Y, Monk AM, Faye L and Li J (2009) Mutations of an alpha1,6 mannosyltransferase inhibit endoplasmic reticulum-associated degradation of defective brassinosteroid receptors in *Arabidopsis*. *Plant Cell* **21**, 3792–3802.
36 Farid A, Malinovsky FG, Veit C, Schoberer J, Zipfel C and Strasser R (2013) Specialized roles of the conserved subunit OST3/6 of the oligosaccharyltransferase complex in innate immunity and tolerance to abiotic stresses. *Plant Physiol* **162**, 24–38.
37 Saijo Y, Tintor N, Lu X, Rauf P, Pajerowska-Mukhtar K, Häweker H, Dong X, Robatzek S and Schulze-Lefert P (2009) Receptor quality control in the endoplasmic reticulum for plant innate immunity. *EMBO J* **28**, 3439–3449.
38 Trempel F, Kajiura H, Ranf S, Grimmer J, Westphal L, Zipfel C, Scheel D, Fujiyama K and Lee J (2016) Altered glycosylation of exported proteins, including surface immune receptors, compromises calcium and downstream signaling responses to microbe-associated molecular patterns in *Arabidopsis thaliana*. *BMC Plant Biol* **16**, 31.
39 Hong Z, Kajiura H, Su W, Jin H, Kimura A, Fujiyama K and Li J (2012) Evolutionarily conserved glycan signal to degrade aberrant brassinosteroid receptors in Arabidopsis. *Proc Natl Acad Sci USA* **109**, 11437–11442.
40 de Oliveira MV, Xu G, Li B, de Souza Vespoli L, Meng X, Chen X, Yu X, de Souza S, Intorne AC, de Manhães AME *et al.* (2016) Specific control of Arabidopsis BAK1/SERK4-regulated cell death by protein glycosylation. *Nat Plants* **2**, 15218.
41 Trempel F, Ranf S, Scheel D and Lee J (2016) Quantitative analysis of microbe-associated molecular pattern (MAMP)-induced Ca^{2+} transients in plants. *Methods Mol Biol* **1398**, 331–344.
42 Maldonado-Bonilla LD, Eschen-Lippold L, Gago-Zachert S, Tabassum N, Bauer N, Scheel D and Lee J (2014) The *Arabidopsis* tandem zinc finger 9 protein binds RNA and mediates pathogen-associated molecular pattern-triggered immune responses. *Plant Cell Physiol* **55**, 412–425.
43 Rentel MC and Knight MR (2004) Oxidative stress-induced calcium signaling in *Arabidopsis*. *Plant Physiol* **135**, 1471–1479.
44 Grubenmann CE, Frank CG, Kjaergaard S, Berger EG, Aebi M and Hennet T (2002) ALG12 mannosyltransferase defect in congenital disorder of glycosylation type lg. *Hum Mol Genet* **11**, 2331–2339.
45 Kobata A (2013) Exo- and endoglycosidases revisited. *Proc Jpn Acad Ser B Phys Biol Sci* **89**, 97–117.
46 Henquet M, Lehle L, Schreuder M, Rouwendal G, Molthoff J, Helsper J, van der Krol S and Bosch D (2008) Identification of the gene encoding the alpha1,3-mannosyltransferase (ALG3) in *Arabidopsis* and characterization of downstream n-glycan processing. *Plant Cell* **20**, 1652–1664.
47 Miyano K and Sumimoto H (2014) N-Linked glycosylation of the superoxide-producing NADPH oxidase Nox1. *Biochem Biophys Res Commun* **443**, 1060–1065.
48 Baer J, Taylor I and Walker JC (2016) Disrupting ER-associated protein degradation suppresses the abscission defect of a weak hae hsl2 mutant in *Arabidopsis*. *J Exp Bot* **67**, 5473–5484.
49 Häweker H, Rips S, Koiwa H, Salomon S, Saijo Y, Chinchilla D, Robatzek S and von Schaewen A (2010) Pattern recognition receptors require N-glycosylation to mediate plant immunity. *J Biol Chem* **285**, 4629–4636.

Supporting information

Additional supporting information may be found online in the Supporting Information section at the end of the article.

Fig S1. Calcium response to osmotic (NaCl) stress is not reduced in the *cce1* mutant.

Fig. S2. Linearity of signal intensities of activated MAPK phospho-forms quantified using the Odyssey Western blot system.

Table S1. (A) List of SNPs found in cce1, which lead to non-synonomous substitution. (B) #Complete list of single nucleotide polymorphisms (SNPs) found in cce1 after Illumina whole genome resequencing.